

Photocatalyst and Photoelectrochemical cell performance of Ag/TiO₂ nanocrystalline thin film under low-intensity visible light

Marwah J. Kadhim^{1*}, M.A. Mahdi¹, J.J. Hassan¹, Salwan K.J Al-Ani²

https://doi.org/10.29072/basjs.20250214

ARTICLE INFO

ABSTRACT

Keywords

Ag/TiO₂, thin-film, photocatalysts, photoelectrochemical cell

Titanium dioxide (TiO₂) nanocrystalline thin films were synthesized using chemical bath deposition (CBD) on glass slides and FTO/glass substrates. Silver (Ag) nanoparticles (NPs) were subsequently deposited onto the surface of the TiO₂ thin films via electrochemical methods. The size of Ag NPs on TiO₂ films ranged from 10 to 79 nm on both glass and FTO substrates. The photocatalytic performance of the Ag/TiO₂ thin films, both untreated and heattreated at 200 °C and 300 °C for 1 h, was evaluated through the photodegradation of methylene blue dye (MB) under white light (0.33 mW/cm²) and sunlight irradiation. Remarkably, TiO₂ thin films heat-treated at 300 °C achieved a degradation ratio of 96% after 240 minutes under white light. Under sunlight and at a pH 10, the degradation ratio reached 100% within 150 minutes. Cyclic voltammetry revealed faradaic behavior in the Ag/TiO₂ thin films. The photoconversion efficiencies (η) of the films, measured in their as-prepared state and after heat treatment at 200 °C and 300 °C, were determined to be 1.5%, 1.6%, and 0.5%, respectively. Mott-Schottky analysis confirmed n-type behavior, indicated a negative shift in the flat band potential (V_{FB}).

Received 28 July 2025; Accepted 28 August 2025, Published 30 August 2025

¹ Department of Physics, College of Science, University of Basrah, Basra, Iraq

² Department of Physics, College of Science, Al-Mustansiriya University, Baghdad, Iraq

^{*}Corresponding author E-mail: marwah.jawad@uobasrah.edu.iq

1. Introduction

Metal oxide nanostructured semiconductor materials such as ZnO, MnO₂, CeO₂, NiO, and titanium dioxide (TiO₂) have gained more interest in various applications, such as photosensors [1], biological, pharmacological fields [2] LEDs [3], gas sensors [4], and dyesensitized solar cells (DSSCs) [5]. Lately, researchers have focused on utilizing these metal oxides for the elimination of organic contaminants, showcasing an effective photocatalytic process for treating polluted water when exposed to ultraviolet UV light [5,6]. Two parameters can limit the efficiency of metal oxide nanostructured compounds in photocatalysis. The first factor is the high recombination rate of electron/hole pairs within the lattice of material. When these pairs recombine before participating in redox reaction process, the overall photocatalytic activity decreases, limiting the effectiveness of the process. Another factor is the high energy band gap of many metal oxide photocatalysts. These materials, like (TiO₂), have a wide optical bandgap that only allows them to absorb in UV light region, which makes up about 5% of the solar spectrum. However, visible light, which makes up about 57% of the solar spectrum, is not effectively absorbed by these materials. This mismatch in light absorption limits their ability to use sunlight fully and reduces photocatalytic performance under sunlight. To overcome these issues, strategies like doping with foreign elements, creating heterojunctions, or designing composite materials are often used. These strategies help enhance charge separation and extend light absorption into the visible range [7, 8]. In addition, metal nanoparticles NPs-semiconductor heterojunction forms Schottky contact at the interface, which is an effective way to enhance e-h separation and improve the efficiency of photocatalytic activity. Thus, decorated noble metal NPs on the TiO₂ surface is a favourable method to decrease the recombination of photogenerated charge carriers and enhance photodegradation activity [9]. Visible light can be used to excitsome metal NPs through the oscillating electric field of the light interacts with electrons in the conduction band [10]. Consequently, these electrons oscillate pronouncedly when the frequency of the input photon approaches that of the collective oscillation of the conduction electrons [9, 10]. The large energygap of 3.2 eV of TiO₂ greatly limits the ability of visible light to be absorbed, resulting in a decrease in its photocatalytic effectiveness [11,12]. In addition, the low quantum efficiency of TiO₂, caused by rapid recombination of photogenerated carriers, is another factor contributing to the decrease in photocatalytic efficiency and hydrogen generation during water splitting [13]. In order to overcome these challenges, it is necessary to modify the broad energygap of TiO₂ by adding of metal nanoparticles on its surface. This

modification will result in a drop in the recombination rate [10]. However, TiO₂ is commonly utilized as a photocatalyst due to its robust catalytic activity and excellent chemical stability [14]. Silver (Ag) NPs are used to modify TiO₂ for photocatalytic applications due to their catalytic activity [15]. Furthermore, the coupling of Ag NPs with TiO₂ is considered a promising way for water splitting under visible light irradiation [16]. The water splitting using photocatalyist depends on the absorbed light with energy that is higher than its energygap to produce electron-hole pairs. The separated excited carriers are moved toward different sites on the surface of the catalyst material to avoid recombination. At these sites, oxidation and reduction of water occur by the photogenerated charge carriers to generate hydrogen and oxygen gas [17]. In this work, TiO₂ was prepared using the CBD method. Then, Ag NPs were deposited on the prepared TiO₂ thin films deposited via an electrochemical method. The photocatalytic performance of the as-prepared Ag/TiO₂ thin film and those annealed were investigated under a pH of 6 and a pH of 10 under the low intensity of white light and sunlight. The properties studied of the PEC cell are based on the Ag/TiO₂ photoelectrode where electrochemical performance and electric properties are measured for Ag/TiO₂ thin film.

2. Experimental part

The structural and morphological characteristics of the thin films were assessed utilizing X-ray diffraction (XRD, X'Pert PROMPDPANalytical) and Field Emission Scanning Electron Microscopy (FESEM, NovananoSEM450, FEI), respectively. Optical properties were examined via UV-Vis spectroscopy (UV1800 Shimadzu). PEC analysis for all thin films was performed using a three-electrode potentiostatic configuration of the CorrTest electrochemical workstation.

2.1 Synthesis of Ag/TiO₂ nanocrystalline thin films

TiO₂ nanocrystalline were deposited using CBD on glass and FTO-glass substrates. Substrates are ultrasonically cleaned using 2-propanol, ethanol, and distilled water (DW). The precursor was prepared using a 4 mL solution of titanium chloride (III) (TiCl₃), 50 mL of DI and 0.1 M of urea (NH₂CONH₂), which was added to fixed the pH at 0.5 [18]. A homogeneous solution with violet color was obtained after stirring RT for 1h. Then, the substrates were vertically immersed inside the beaker containing the above precursor, and the temperature of the solution was increased to 55 °C for 3 hours. Then, the prepared samples were washed with distilled water, followed by annealed at 350 °C for 1 hour to enhance the crystal structure and evaporate the remaining unwanted

materials. Ag/TiO₂ nanocrystalline thin films were fabricated by immersing the prepared TiO₂ thin films in Ag NP solution for 5 h within an electrochemical process using two pure silver electrodes in 100 mL distilled water. After the power was turned off, the TiO₂ thin film samples were left in the solution for 19 hours at room temperature. Then, Ag/TiO₂ nanocrystalline thin films are dried, and other samples are annealed at 200 °C and 300 °C for 1 h. The surface morphology was investigated using Field-Emission Scanning Electron Microscope (FESEM) type NOVA nano 450 SEM, and optical properties were measured through UV-vis spectroscopy using 1800 Shimadzu equipment to evaluate absorption spectra and energygap of Ag/TiO₂ nanocrystalline thin films and the degradation ratio of MB dye solutions.

2.2 Photocatalytic measurements

Photocatalytic measurements of prepared Ag/TiO₂/glass nanocrystalline thin films and for samples annealed at 200 °C and 300 °C for 1 h were investigated by an aqueous solution containing 0.005 M of MB dye. The prepared Ag/TiO₂/glass nanocrystalline thin film is placed inside a beaker containing 40 ml solution of MB dye and illuminated by 0.33 mW/cm² of white light with various values of pH (6 and 10) and exposure times of 30–240 min. The pH of the MB dye solution was justified using NaOH and some drops of HNO₃ acid. However, the pH control the surface charge of the photocatalyst which makes the photocatalyst positively charged in an acidic medium and negatively charged in a basic medium [19]. The acidic medium was represented by a pH of 6 while the basal media was represented by a pH of 10.

2.3 Photoelectrochemical measurements

The photoelectrochemical cell (PEC) contains three electrodes: a counter electrode constructed of a platinum plate with a dimension of (1×1) cm, a working electrode with a dimension of 1.5×2.5 cm, and a reference electrode constructed of Ag/AgCl (KCl saturated). The electrolyte was a KOH solution with 1.0M and pH of 13.6 under irradiation by 0.33 mW/cm² of white light. Cycle voltammetry (CV) was performed to estimate the PEC efficiency under dark conditions, while linear sweep voltammetry (LSV) measurement was performed under dark and light conditions to measure the J-V characteristic with a different scan rate of 0.05-0.5 V/s

3. Results and discussion

3.1 Optical properties

Figure 1A shows the optical absorption spectra of prepared Ag/TiO₂ nanocrystalline thin films as well as after being heated to 200 and 300 °C, which appear at 367, 446, and 379 nm, respectively. The absorbance visible light isf due to the surface plasmon resonance (SPR) effect of Ag NPs prepared on the surface of TiO₂ thin films [20]. SPR events and the synchronized oscillation of free electrons in resonance with incident photons boost photocatalytic effectiveness by increasing light absorption and scattering, as well as causing separation of charge in semiconductors. Nonetheless, a Schottky connection can be established between metallic nanoparticles and semiconductors. The equilibrium alignment of the Fermi levels between metal and semiconductor materials generates a built-in electric field in the space-charge region adjacent to the interface, facilitating the separation of photogenerated charge carriers [17]. The energygap Ag/TiO₂ nanocrystalline thin film prepared onto glass substrates and those annealed at 200 and 300 °C are 3.38, 2.78, and 3.27 eV, respectively, as shown in Fig. 1B. These values are associated with the rutile phase of TiO₂ [4, 6, 13]. However, the decreasing energy gap with increasing annealing temperature could be because the samples contain mixed phases of rutile and anatase [6, 13]. As shown in Fig. 2A, peaks of absorbance spectra-for as-prepared Ag/TiO₂/FTO-glass nanocrystalline thin films annealed at 200 °C and 300 °C appear at 364, 400, and 464 nm, respectively. The high absorbance value in the visible region could be due to the SPR effect of Ag-NPs that covered the surface of TiO2 nanocrystalline thin films. The energygap value of Ag/TiO₂/FTO-glass nanocrystalline thin films and those annealed at 200 °C and 300 °C are 3.40 was 3.10, and 2.67 eV, respectively as shown in Fig. 2B. According to Singh et al. [21], the reduction in energygap value for annealed samples is could be the density change of film after the structure phase transition [21].

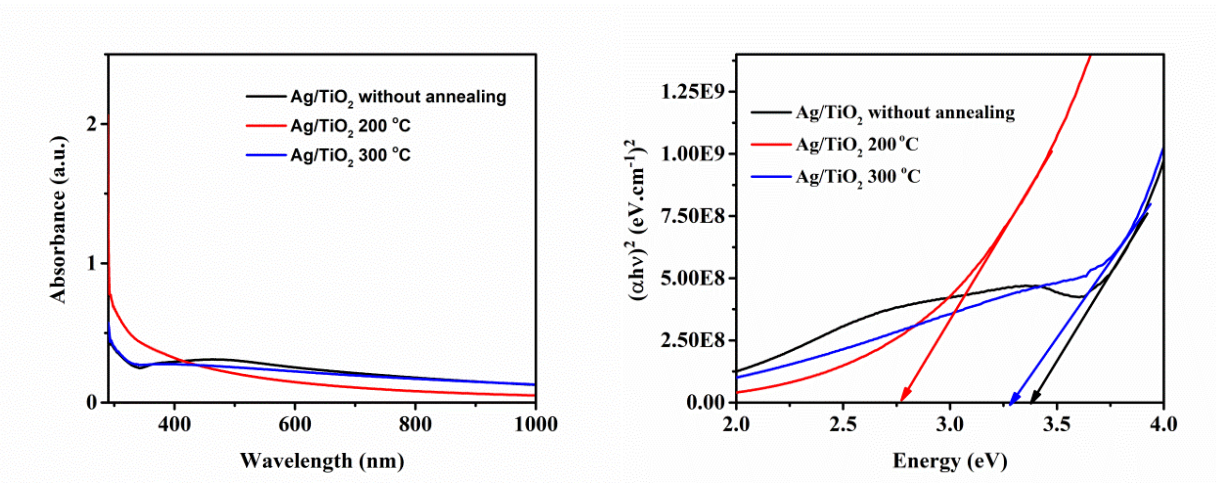


Fig. 1: (A) The absorbance spectrum of Ag/TiO_2 nanocrystalline thin films grown onto glass substrates and (B) $(\alpha h \upsilon)^2$ vs. photon energy plot for $Ag/TiO_2/glass$ nanocrystalline thin films.

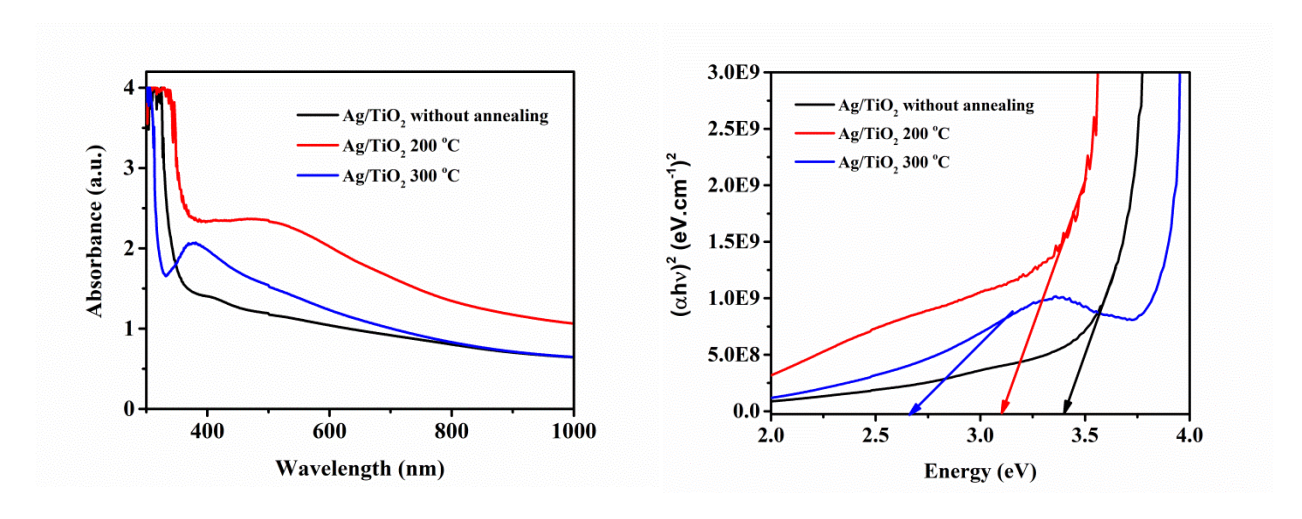


Fig. 2: (A) The absorbance spectrum Ag/TiO₂ nanocrystalline thin films grown on FTO substrate and (B) $(\alpha h \upsilon)^2$ vs. photon energy plot of Ag/TiO₂/FTO nanocrystalline thin films.

3.2 Surface morphology and structural properties

Figures 3A and 3B show the FESEM images of the Ag/TiO₂ thin films prepared onto FTO/glass and glass substrates. Figure 3A shows the Ag NPs that were deposited onto TiO₂/glass thin films, and the particle size of the NPs was calculated to be 10–79 nm using the ImageJ program. TiO₂ thin film that grew onto glass substrates was formed as a semi-flower with semi-plate corollas having a length of 29.6-99 nm and width of 14.2-69.6 nm covered by Ag NPs. Figure 4A shows

the XRD pattern of prepared Ag/TiO₂ thin films deposited onto glass substrates. TiO₂ thin film appeared with two diffraction peaks at 36.6° and 44.2° which correspond to the crystal planes of (101) and (210) of Rutile phase (JCPDS Card no. 00-02-03873), whereas the samples that annealed at 200 °C showed peak at 54.4° which corresponds to (211) plane. However, annealing prepared thin films at 300 °C, led to the appearance of a single diffraction peak at 44.06° related to the rutile phase in addition to other three peaks at 25.75°, 37.9°, and 48.37 corresponding to (101), (004), and (200) of anatase phase planes (JCPDS card no. 01-078-1508), respectively. The XRD patterns of prepared Ag/TiO₂ thin film onto FTO/glass substrate are shown in Fig.4B. The distinct peak can be observed in the XRD patterns at 37.8° of as-prepared Ag/TiO₂ thin films and those annealed which are related to (004) of the anatase phase. Moreover, the Ag/TiO₂ thin films annealed at 200 °C show a peak at 25.03° which corresponds to the (101) plane of anatase. Further, two peaks have noted at 27° and 52° corresponding to (110) and (220) crystalline planes of FTO substrate, respectively according to JCPDS NO.77-0452 [22]. In Figs. 4A and 4B, two diffraction peaks are shown at 38° and 43.8° corresponding to the (111) and (200) plane of Ag metal according to JCPDS NO. 04-0783 [23]. Meanwhile, the two peaks of AgO at 32° and 46.5° correspond to (202) and (132), which agrees with JCPDS NO. 84-1108 [24].

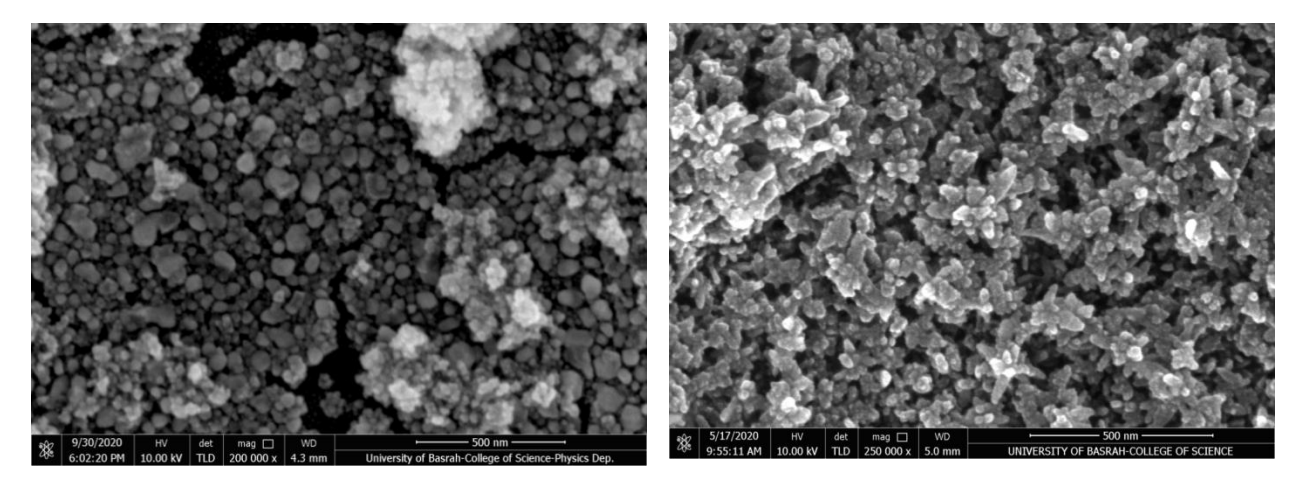


Fig.3: FESEM image of the Ag/TiO₂ nanocrystalline thin films grown on: (A) glass substrates (B) FTO/glass substrates.

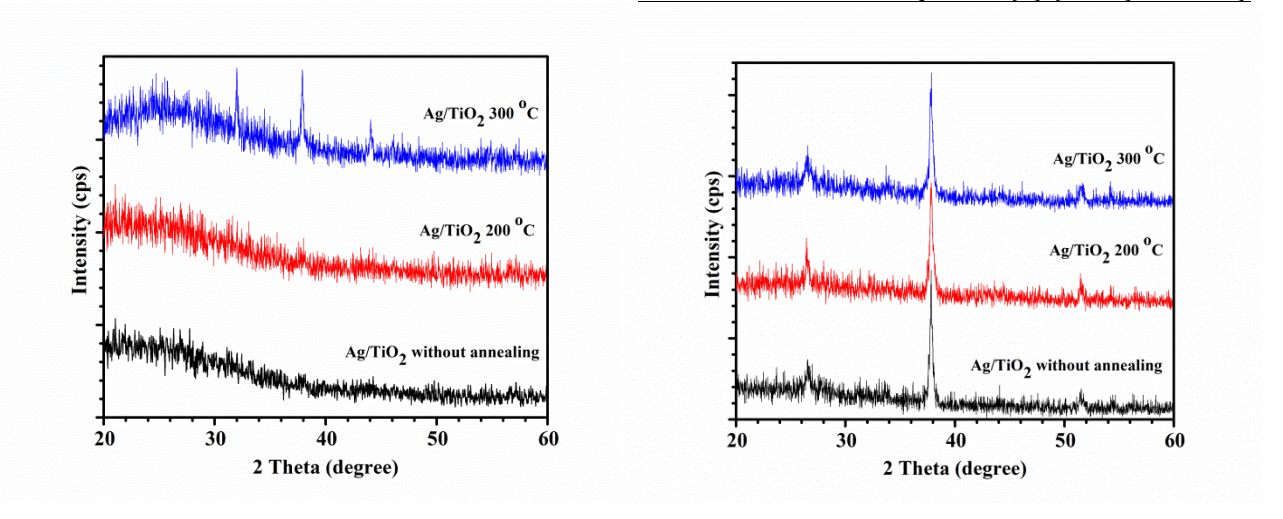


Fig.4: XRD patterns of the Ag/TiO₂ thin films grown on (A) glass substrates (B) FTO/glass substrates.

3.2 Photocatalyst activity

The absorbance spectra of MB dye, which were catalyzed by the as-prepared Ag/TiO2 nanocrystalline thin film and those annealed at 200 and 300°C, are displayed in Figures 5A, 5B, and 5C. The measurements were made at a pH of 6 under 0.33 mW/cm² intensity of white light with varying exposure durations of 30 to 240 minutes. Figures 6A, 6B, and 6C are the absorbance of MB dye measured with a pH value of 10 for the samples under the same conditions. The absorption peak decreases with an increasing irradiation time of all samples indicating for degradation of MB dye. The degradation ratio of the MB dye was calculated using the formula [25]:

Degradation rate(%) =
$$\frac{A_{\circ} - A}{A} \times 100$$
,

where A_o represents the absorbance value before exposure, and A represents the absorbance value after exposure to light. Figures 7A and 7B show the degradation rate vs. irradiation time of the preparedAg/TiO₂ thin films and annealed samplesusing pH of 6 and 10, respectively. The degradation rate when the pH is 10 (basal medium) is higher than that when the pH is 6. In the basal medium, increasing hydroxyl ions in the MB solution leads to the form of hydroxyl radicals OH^{\bullet} that in turn leads to an increase in the photodegradation of the MB dye on the catalytic material surface [23, 24]. The degradation rate of MB dye with pH of 6 that was irradiated by a white light for 240 min by prepared Ag/TiO₂ nanocrystalline thin films and samples annealed at 200 °C and 300 °C was 68%, 59%, and 56%, respectively. However, when the pH was 10, the

samples appeared degradation rates of 85%, 92%, and 96%, respectively after 240min of irradiation by 0.33 mW/cm² intensity of white light. The prepared Ag/TiO₂ thin films and annealed samples at 300 °C show higher photocatalytic activity than the other samples which could be due to the annealing process leading to converting the rutile phase of TiO₂ to anatase. In addition, the photocatalysis by mixed phases of TiO₂ is better than that obtained by the rutile phase. The conduction band of the anatase phase is greater than that of the rutile phase, causing the transfer of generated electrons from the anatase to rutile TiO₂ while holes are transferred from the rutile to the anatase and prevent recombination of charge carriers [28]. P. Sangpour et al. evaluated the photocatalytic activity of Ag/TiO₂ nanostructure through the degradation of MB dye under white light irradiation and obtained an efficiency of 75% after 200 min of exposure [29].

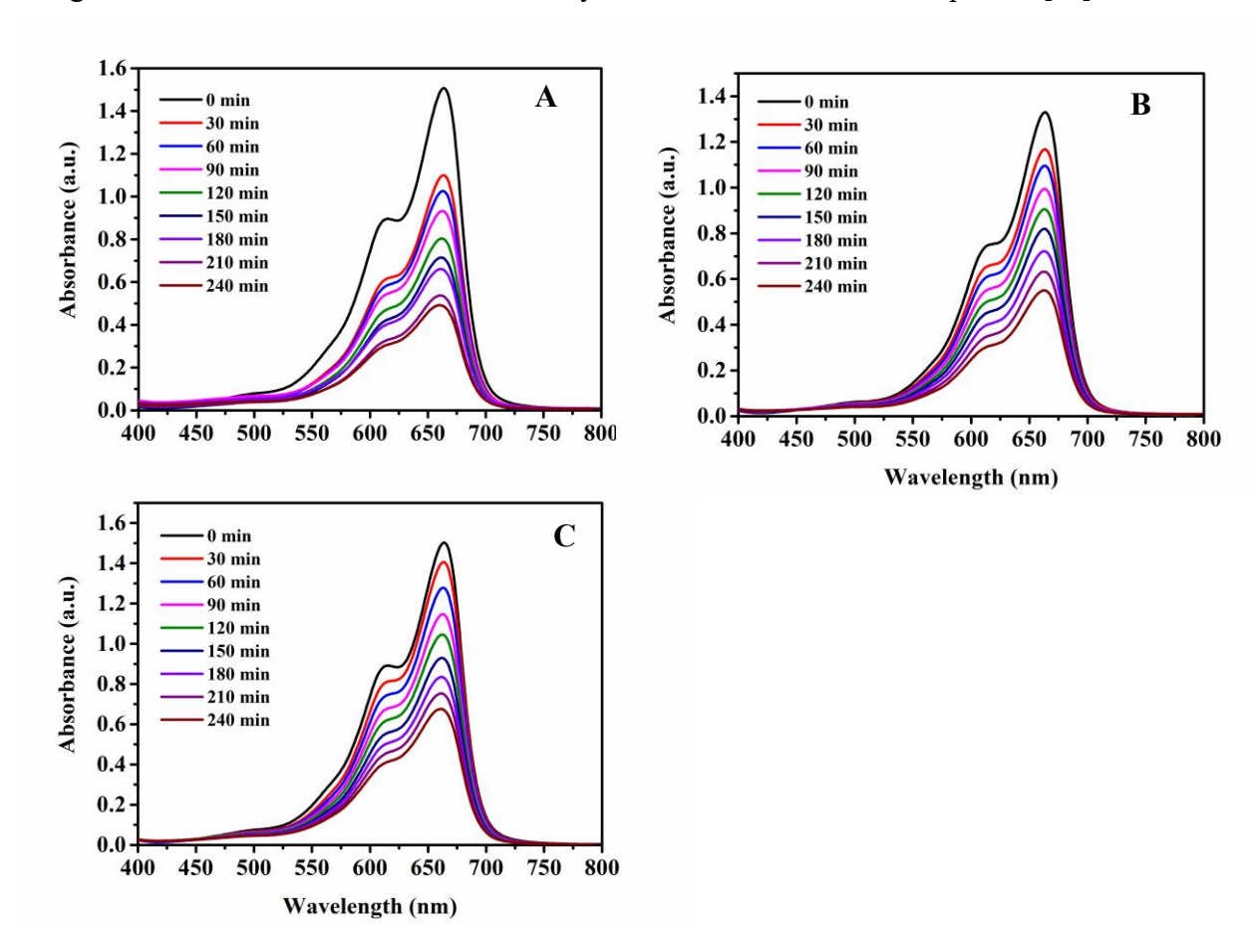


Fig.5: Absorbance spectra of MB dye under the different times of visible light irradiation with pH of 6 of Ag/TiO₂ thin films of (A) as prepared, (B) annealed at 200 °C (C) annealed at 300 °C

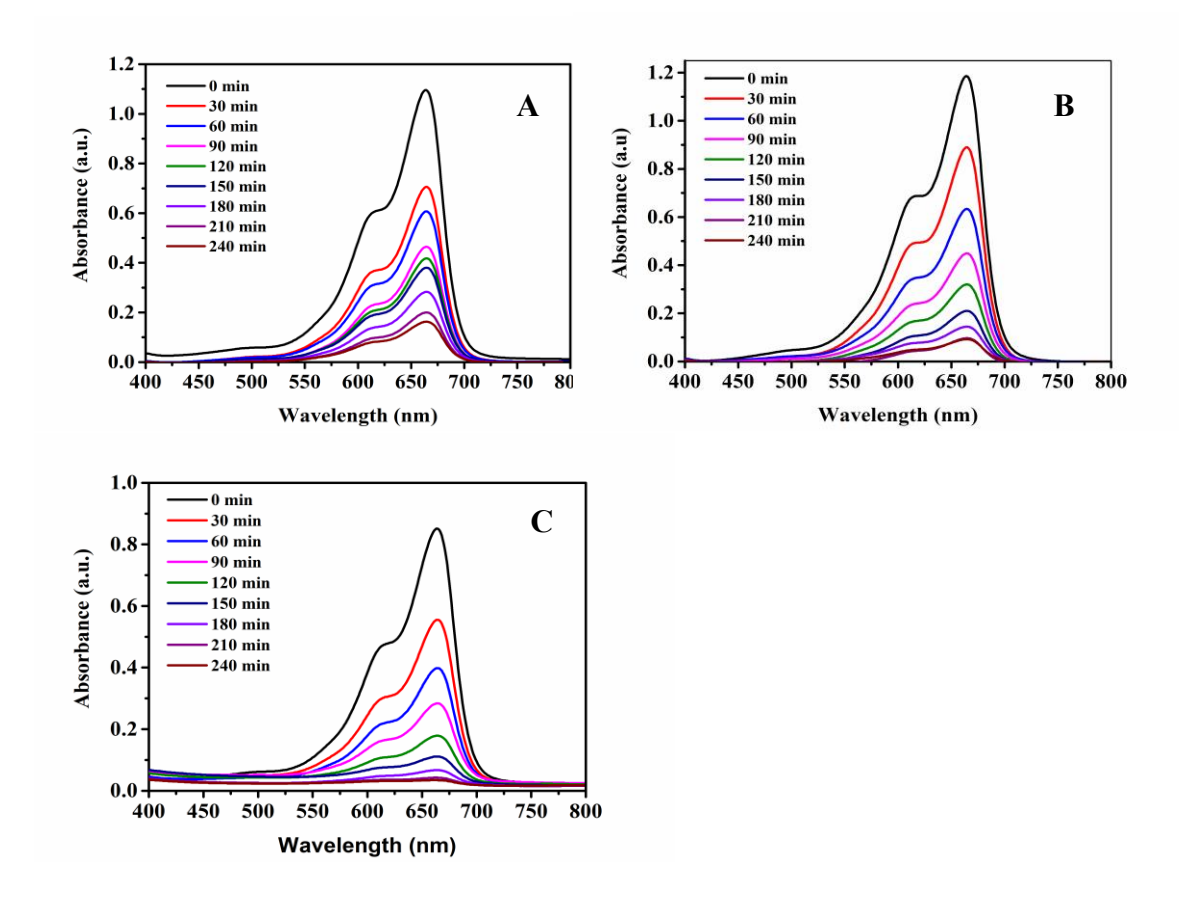


Fig.6: Absorbance spectra of MB dye under the different times of visible light irradiation with pH of 10 of Ag/TiO2 thin films of (A) as prepared, (B) annealed at 200 $^{\circ}$ C (C) annealed at 300 $^{\circ}$ C.

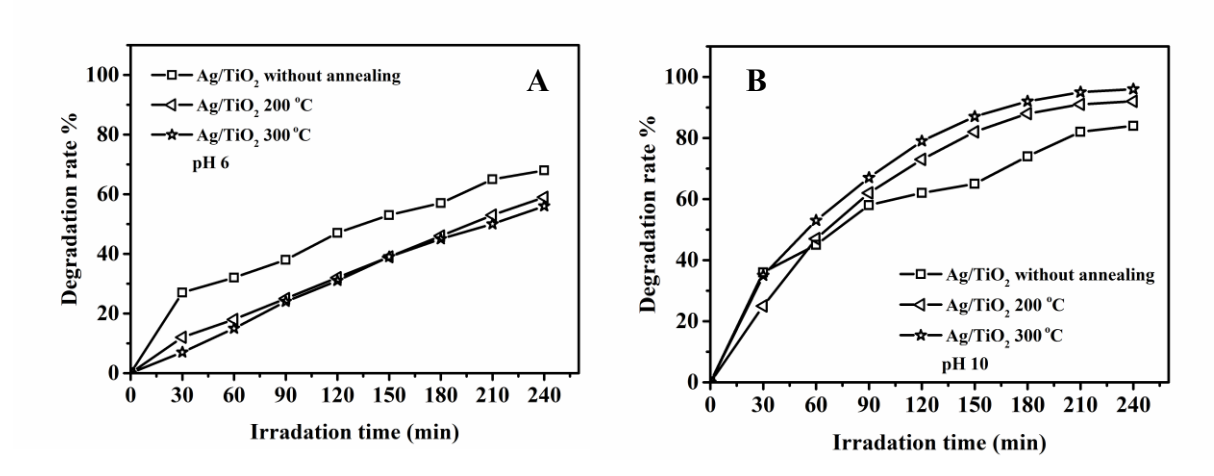


Fig.7: MB dye degradation rate vs. irradiation time for Ag/TiO₂ thin film with (A) pH of 6 and (B) pH of 10 under white light.

The kinetic rate of the MB dye can be estimated by the first-order Langmuir relation formula [27, 28]:

$$C = C_0 e^{-kt}, 2$$

where C_0 and C are the concentration of the MB dye before and after treatment, respectively, t is the time of the reaction and k is the kinetics rate of the degradation reaction. The kinetic rate value for the MB dye with a pH of 6 is 0.0044, 0.0036, and 0.0039 min⁻¹ for the as-prepared Ag/TiO₂ nanocrystalline thin films and annealed samples at 200 °C and 300 °C, respectively increased to be 0.0073, 0.0114, and 0.0138 min⁻¹ for the same samples when pH value was 10. The optical absorbance spectra of the MB dye solution catalyzed by as-prepared Ag/TiO₂ nanocrystalline thin film and annealed samples with pH of 6 under sunlight and exposure time of 30-240 min are shown in Figs. 8A, 8B, and 8C. The absorbance spectra for the MB dye solution for pH of 10 that was catalyzed by the -prepared Ag/TiO₂ thin film and annealed samples at 200 °C and 300 °C under sunlight are shown in Figs. 9A, 9B, and 9C. However, the absorbance value of MB dye is reduced when the illumination time is increased for all prepared samples. Thus, the degradation rate increases with increasing illumination time and pH value for all MB dyes that are catalyzed by as-prepared and annealed TiO₂ nanocrystalline thin films (Figs. 10A, and 10B). The sample TiO₂ thin film annealed at 300 °C showed a degradation rate of 100% after 150 min of sunlight irradiation with a pH of 10. T. Ngoc et al. evaluated the photocatalytic activity of Ag/TiO₂ nanotube through MB dye degradation under the effect of sunlight and obtained an efficiency of 96% after 20 min of irradiation [32] while A. Shet and V. S. K were getting a photodegradation ratio of Ag/TiO₂ core-shell through phenol dye under sunlight are 70% after 360 min [33]. Singh et al. reported that the Photocatalytic Activity of Ag-TiO₂ Hybrid Plasmonic Nanostructures is 97 % of 10 µM MB at 60 min [34], whereas Aravind et al. [35] mentioned a degradation rate of 94% in 120 min by using Ag-TiO₂ nanofibers by synthesies the hydrithermal method as a catalyst under natural sunlight, but the intensity of sunlight was not mentioned [35]. Preethi et al. [36] studied RB degradation using Cd₂SnO₄ microcrystals in cubic and orthorhombic phase catalysts at 120 min and showed degradation of 91% and 82%, respectively. Koppala et al. [37] defect-SnO₂ under UV irradiation exceeded 80% degradation of RB in 120 min. The same condition for the previous study, except for the use of visible light and ZnO-Ag NPs [38]. In the case of this work, Ag NPs ability for absorb visible light incident and induce coherent collective oscillation of electrons, which in turn produces e with high kinetic energy in the region of 1 to 3 eV, is known as plasmonic

photocatalysis [39]. Consequently, highly energetic electrons produced by this process transfer from surface metal NPs toward TiO₂, these electrons called "hot electrons" have energy greater than the higher Schottky barrier wherefore TiO₂ accepts the hot electron because the conduction band has of state density of high Hot electron transfer leaves behind holes by doing an internal electric field hence stopping recombination so the electrons are concentrated on the TiO₂ surface close to the Ag NPs [39]. Particularly, the fermi levels in TiO₂ CB highest than most metals noble which leads to suppressing (e⁻-h⁺) recombination so the material's ability to absorb visible light is improved by the surface plasmon resonance (SPR) action of Ag [40]. The charge carriers produced a reaction with the adsorbed H₂O and O₂ molecules and highly reactive superoxide O₂⁻ and hydroxyl radicals OH eventually. Hence, the Photodegradation of dye under visible light returns to these radicals [40, 41] as shown in schematic 1. The kinetic rate at pH of 6 was 0.0055, 0.0098, and 0.0055 min⁻¹ for the prepared Ag/TiO₂ thin films and samples annealed at 200 °C and 300 °C under sunlight irradiation for 240min, whereas the kinetic rate became 0.0371, 0.0344, and 0.0334 min⁻¹ for the same samples at pH of 10. Sunlight irradiation causes the transfer the electrons generated by light from Ag NPs to the conduction band of TiO₂ through the Schottky junction. The SPR of metal NPs causes the creation of a highly intense electric field around Ag NPs where transferred plasmon resonance energy increases the concentration of charge carriers in the Ec and Ev bands of TiO₂. The photogenerated electrons that interact with the surface of oxygen molecules to form superoxide radicals (•O₂⁻). When adsorbed H₂O molecules react with holes in the Vb of TiO_2 form extremely reactive hydroxyl radicals (OH^{\bullet}), and these ${\bullet}O_2$ and OH^{\bullet} interact with MB and led to degrading dye [13].

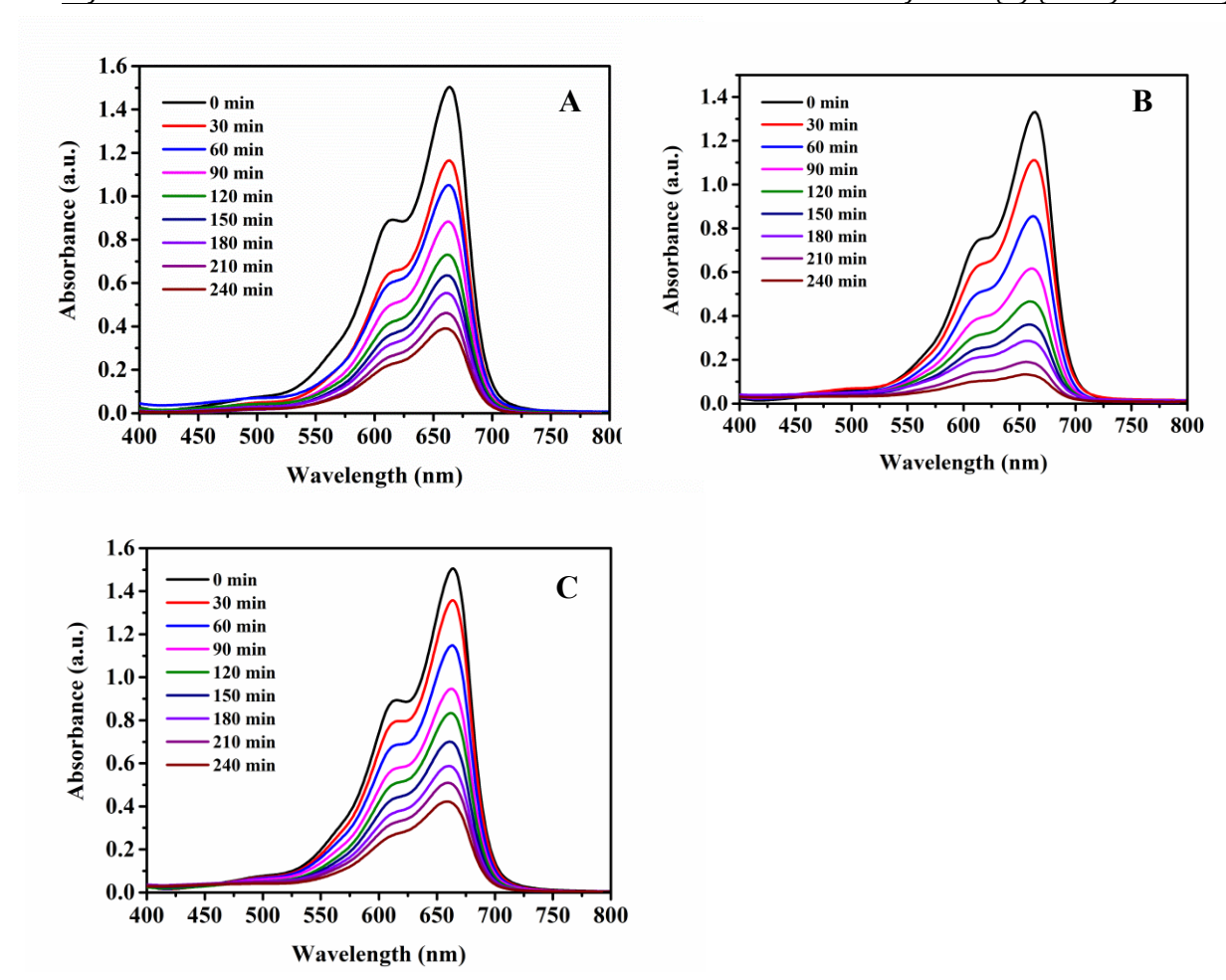


Fig.8: Absorbance spectra of MB dye with pH of 6 under the different times of sunlight irradiation of Ag/TiO₂ thin films (A) as prepared, (B) annealed at 200 °C, and (C) annealed at 300 °C.

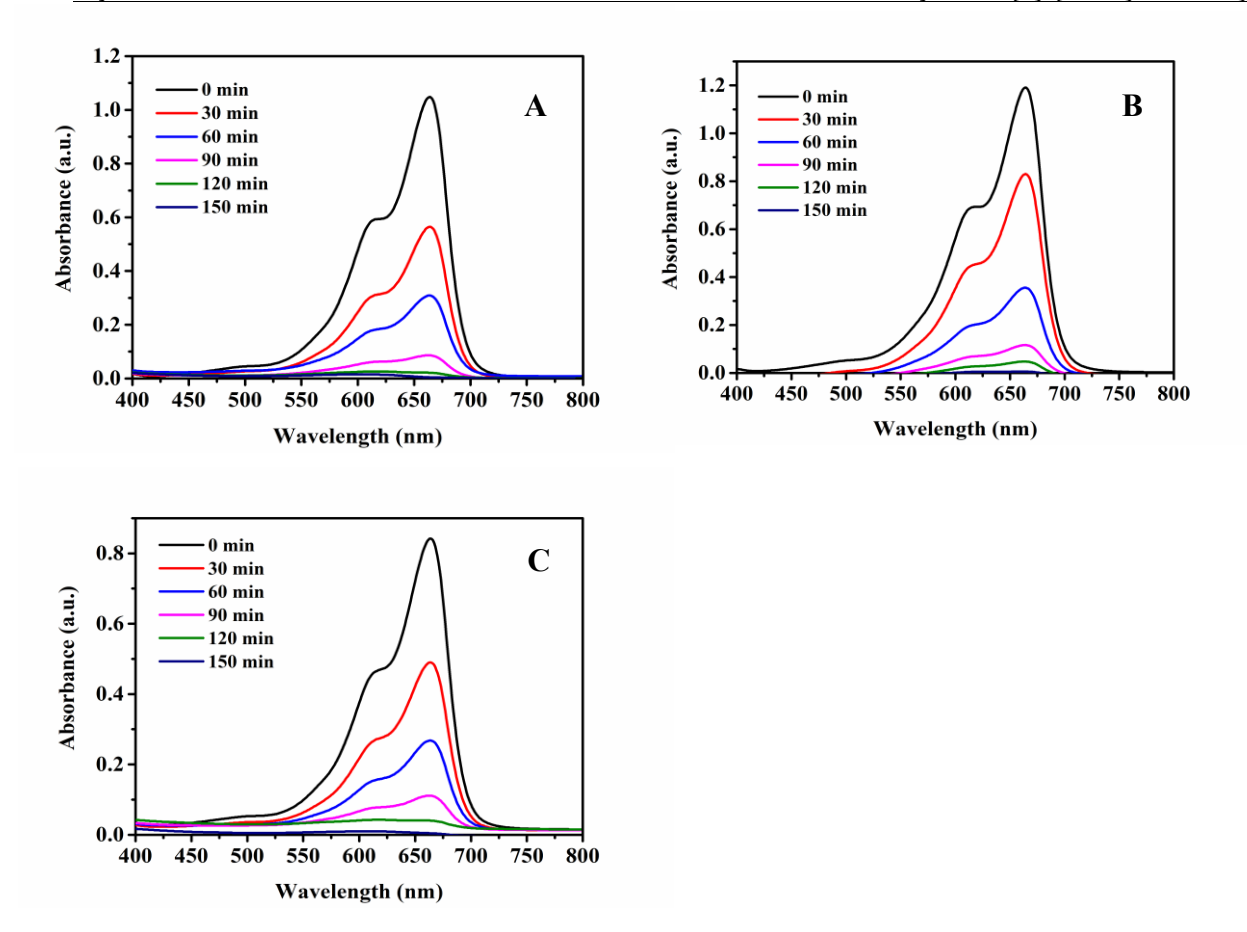


Fig.9: Absorbance spectra of MB dye using pH of 10 under different time of sun light irradiation of Ag/TiO₂ thin films (A) as prepared, (B) annealed at 200 °C and (C) annealed at 300 °C.

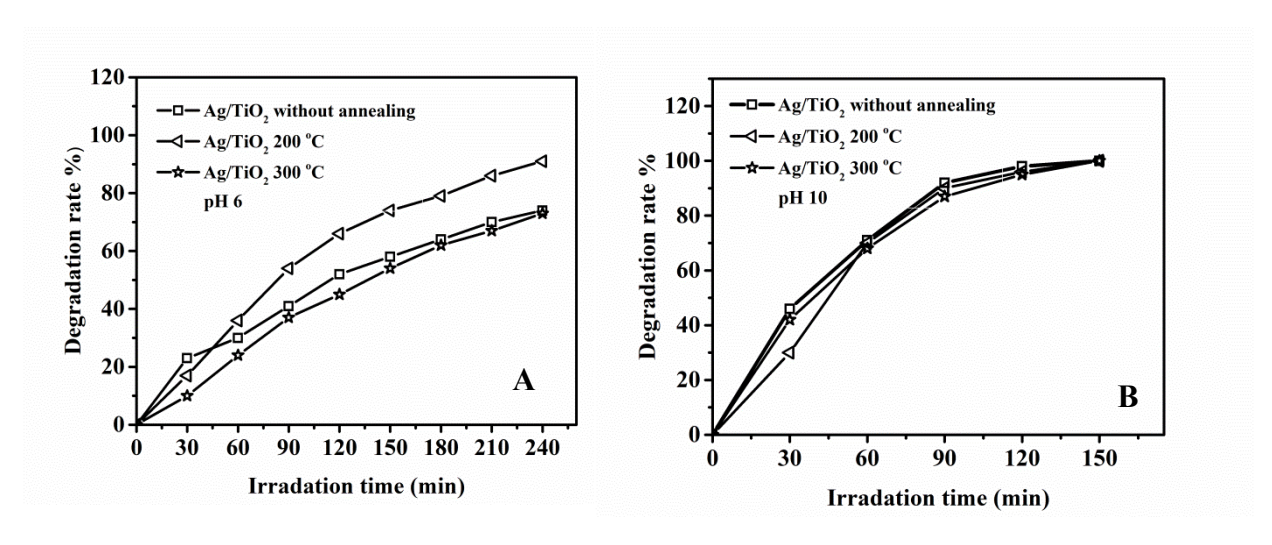


Fig.10: MB dye photodegradation rate vs. irradiation time for Ag/TiO₂ nanostructured thin films with (A) pH of 6 and (B) pH of 10.

Figures 11A, 11B, and 11C show the CV of the prepared Ag/TiO₂, nanocrystalline thin films electrode, and those annealed at 200 and 300 °C at different scan rates, respectively. The asprepared samples and samples annealed at 200 °C exhibit a faradaic reaction where anodic and cathodic peaks of Ag/AgCl appear at 0.39 and 0.0 V, respectively (Figs. 11A and 11B) while Ag/TiO₂ nanocrystalline thin film that annealed at 300 °C exhibits an irregular cathodic peak as shown in Fig. 11C. According to last publised work [43], the absence of reduction and oxidation peaks is due to several causes including rapid redox reaction, short lifetime of separations, reversibility, and good electrical conductivity which cause the electric coupling of redox sites. The areal capacitance *C_s* is described in the following relationship [44]:

$$C_s = \frac{area\ under\ cycle}{2SV\Delta V}$$

where S, V, and ΔV are the photoelectrode area, scan rate, and electrolyte potential window, respectively. Figure 12 shows that the areal capacitance reduction (Cs) vs. scan rate ranges from 0.05 V/s to 0.5 V/s for Ag/TiO₂ thin films. The Cs value for as-prepared Ag/TiO₂ thin films and samples annealed at 200 °C and 300 °C were 709, 347, and 2866 F/cm², respectively. This decreases values of area capacitance with increasing scan rate because of the slow ion diffusion that led to a quick reduction of ion concentration on the photoelectrode surface [45]. However, the area of the electrode's inner surface plays a significant role in this process; in particular, the lower surface area is implicated in electrochemical activities at a fast scan rate [45]. The photoconversion efficiency (η) of Ag/TiO₂ nanocrystalline thin films under irradiation by white light at 0.1 V applied bias vs. Ag/AgCl is calculated evaluated through [46]:

$$\eta = \frac{J_{ph} \times (1.23 - V_b)}{P_{total}} , \qquad 4$$

where J_{ph} is the photocurrent density, P_{total} is the power density of photon illumination, and V_b is applied voltage versus hydrogen reference electrode. The η value of the as-prepared Ag/TiO₂ nanocrystalline thin films is 1.5, whereas the samples annealed at 200 °C and 300 °C are 1.6 and 0.5, respectively. However, I.S. Cho et al. obtained η of 0.17 for TiO₂ NRs at 0.65 V vs. Pt electrode [47]. Otherwise, Raja et al [48] reported that TiO₂ nanotubular arrays annealed at 350°C for 6 hours in a nitrogen environment exhibited a peak photo conversion efficiency of approximately 4% in 1M KOH electrolyte and around 3% in a 3.5wt.% sodium chloride solution.

The flat band potential (V_{FB}) of the photoelectrode and the charge carrier density (N_D) for the photoanode were determined using the Mott–Schottky plot under dark conditions. The semiconductor–liquid junction interfacial capacitance can be described by [49]:

$$\frac{1}{C^2} = \frac{2}{e\varepsilon\varepsilon_0 N_D} \left(V_A - V_{FB} - \frac{KT}{e} \right)$$
 5

where C is the capacitance of the space charge (F/cm²), ε_0 is vacuum permittivity, ε is the dielectric constant of TiO₂ (41.4 for anatase and 154.2 for rutile) [50], V_A is applied potential, e is the electron charge, T is temperature, and K is Boltzmann constant and Mott–Schottky preferred measurement in dark conditions. The N_D and V_{FB} are important factors for semiconductors that affect the charge transport and onset potential, which consequently affect the PEC performance [49, 50].

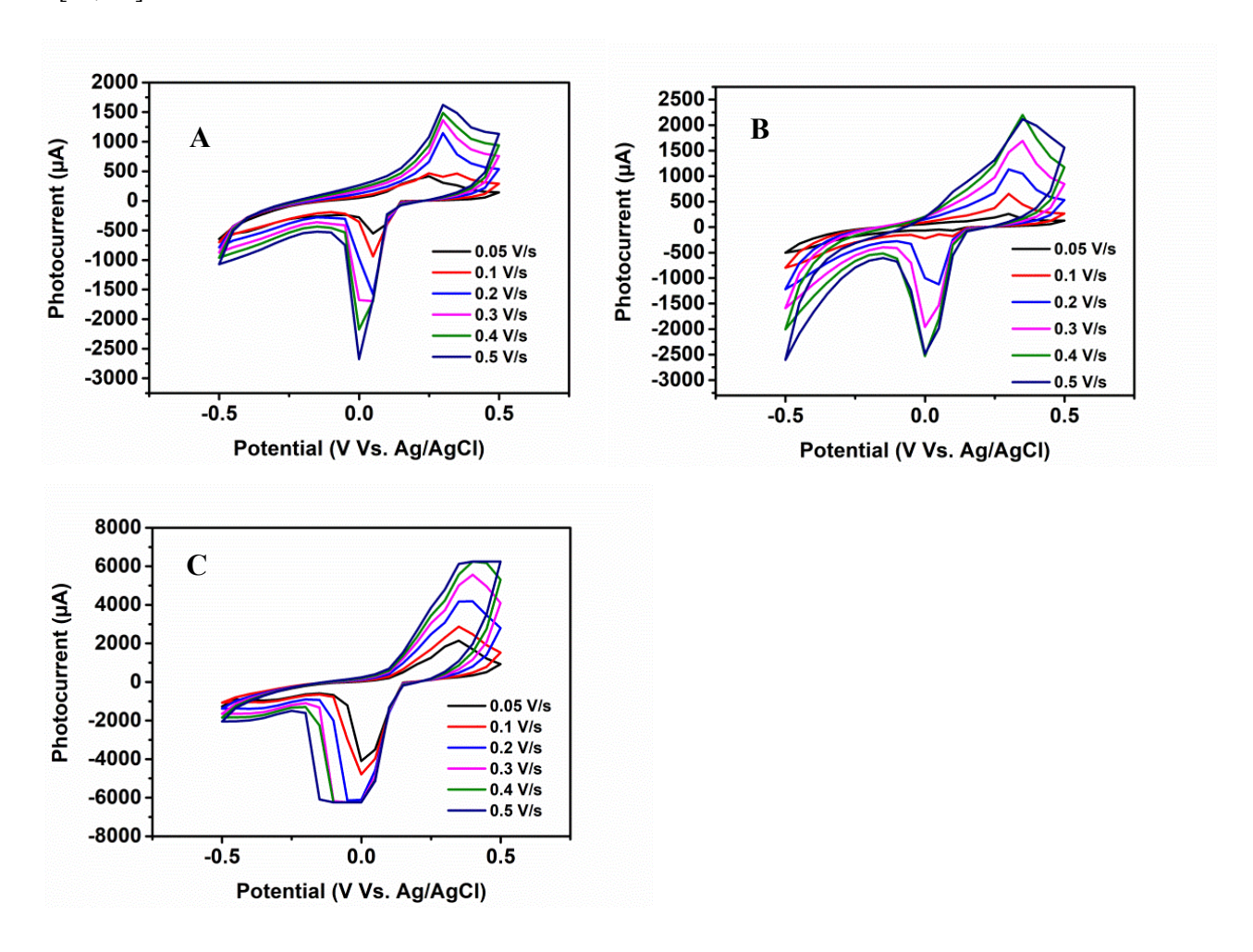


Fig. 11: CV of the Ag/TiO₂ nanocrystalline thin films electrode with various scan rates (A) as prepared (B) annealed at 200 °C (C) annealed at 300 °C

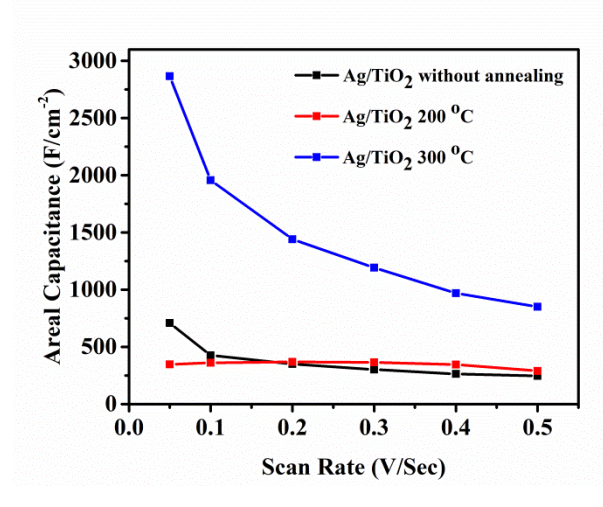


Fig. 12: Areal capacitance of Ag/TiO₂/FTO/glass nanocrystalline thin films photoelectrodes with various scan rates.

Figures 13A, 13B, and 13C represent the Mott-Schottky plots of prepared and annealed Ag/TiO₂ nanocrystalline thin films at frequencies values of 100, 1000, and 10000 Hz, respectively. The Mott-Schottky behavior of all samples is nonlinear indicating that the three assumptions mentioned in Eq. 5 are not fulfilled. However, good linearity appears at the interval of -0.2 to 0.5 V versus Ag/AgCl applied bias when the frequency is 100 Hz. The calculated V_{FB} potential was -0.17, 0.27, and -0.32 V for the as-prepared Ag/TiO₂ nanocrystalline thin films and samples leat treated at 200 °C and 300 °C, respectively. The calculated N_D value for 100 Hz is 9.6×10²¹, 1.1×10²², and 9.4×10²¹ cm⁻³ for the as-deposited Ag/TiO₂ nanocrystalline thin films and those annealed at 200 °C and 300 °C, respectively. The V_{FB} value at the frequency of 1000 Hz is -0.18, -0.27, and -0.32 V for the nanocrystalline thin films and samples heat treatments at 200 °C and 300 °C, respectively, and the N_D value of the same samples was 4.1×10^{21} , 4.9×10^{21} , and 4.7×10^{21} cm⁻³, respectively. Furthermore, the V_{FB} value of the prepared Ag/TiO₂ nanocrystalline thin films and samples heat treated at 200 °C and 300 °C are -0.03, -0.08, and -0.15 V, respectively, under the frequency of 10 000 Hz while the N_D value of the same samples is 1.0×10^{21} , 1.1×10^{21} , and 9.5×10²⁰ cm⁻³, respectively. However, found that the N_D value of prepared samples decreases when the frequency increases which can be ascribed to the contribution of surface states to the capacitance [26]. Increasing donor density refers to the extent of band bending at the semiconductor surface, which boosts charge separation efficiency and subsequently improves photocurrent density under irradiation [27]. Donor density is a remarkable parameter for metal oxides where the excess donor concentration converts the semiconductor into metallization, which is a conductor material of the semiconductor. Metallization reduces the width of the depletion region (W) and the

field, thereby decreasing the photocurrent density [26]. D.R. Ortega et al. found that the N_D is 3.11×10^{22} cm⁻³ for TiO₂ NPs with homogeneous distribution and agglomerate structure with a globular shape [53]. These results are comparable with the findings of T. H. Lee et al. that the N_D is 6.9×10^{20} cm⁻³ for TiO₂ NRs synthesized via CBD under 1 kHz and applied potential of -0.7–0 V (vs. SCE) [54]. All obtained values of V_{FB} are negative indicating that the photoanode electrode is performing better because of the charge separation ease of photogenerated electron/hole pairs, thereby improving the water-splitting performance [55].

The depletion region (W) of interface between semiconductor and electrolyte interface can be computed using the relationship [49]:

$$W = \left(\frac{2\varepsilon\varepsilon_0(V - V_{FB})}{eN_D}\right)^{1/2}$$

The calculated W values when the frequency is 100 Hz are 0.69, 0.76, and 0.87 for the as-prepared Ag/TiO₂ nanocrystalline thin films and those annealed at 200 °C and 300 °C, respectively. When the frequency is 1000 Hz, the W values are 1.07, 1.13, and 1.23 nm for the same samples and increased to 1.46, 1.67, and 2.12 nm under a frequency of 10000 Hz.

The diffusion lengths of electrons and holes or Debye length (L_D) for the photoelectrode can be calculated using the equation [56]

$$L_D = \left(\frac{\varepsilon \varepsilon_0 kT}{e^2 N_D}\right)^{1/2}.$$

Hence, the L_D at 100 Hz is (2, 1.4, and 1.5) $\times 10^{-8}$ cm of the prepared Ag/TiO₂ nanocrystalline thin films and for those annealed. Increasing the frequency to 1000 Hz decreases the L_D to (2.3, 2.1, and 2.2) $\times 10^{-9}$ cm for the as-prepared and annealed samples, respectively. At a frequency of 10000 Hz, the L_D value increases to 5×10^{-8} cm for the prepared and heat treated Ag/TiO₂ nanocrystalline thin films. The Fermi level (E_F) can be calculated from the equation [57]

$$E_F = -eV_{FB}$$

The maxima E_{VB} and minima E_{CB} can be determined using the following equations:

$$E_{CB} = E_F - kT \ln \left(\frac{N_D}{N_C} \right)$$

$$E_q = E_{CB} - E_{VB}$$

The obtained Mott–Schottky parameters, Fermi energy (E_F), conduction band, and valance band of all prepared and annealed Ag/TiO₂ nanocrystalline thin films at frequencies of 100, 1000, and 10000 Hz are listed in Tables 1, 2, and 3, respectively. Furthermore, the deposition of Ag onto the surface of TiO₂ nanocrystalline thin films increases the efficiency of photogenerated charge carrier separation and faster charge transfer at the solid/liquid photoelectrode interface and prevents the recombination of charge carriers. This phenomenon is led to an increase in the concentration of photogenerated charge carriers where the photogenerated electrons can fast transfer to the oxygen absorbed on the TiO₂ surface [58]. However, the effect of annealing on the photoelectrode properties did not appear significantly due to the low temperature.

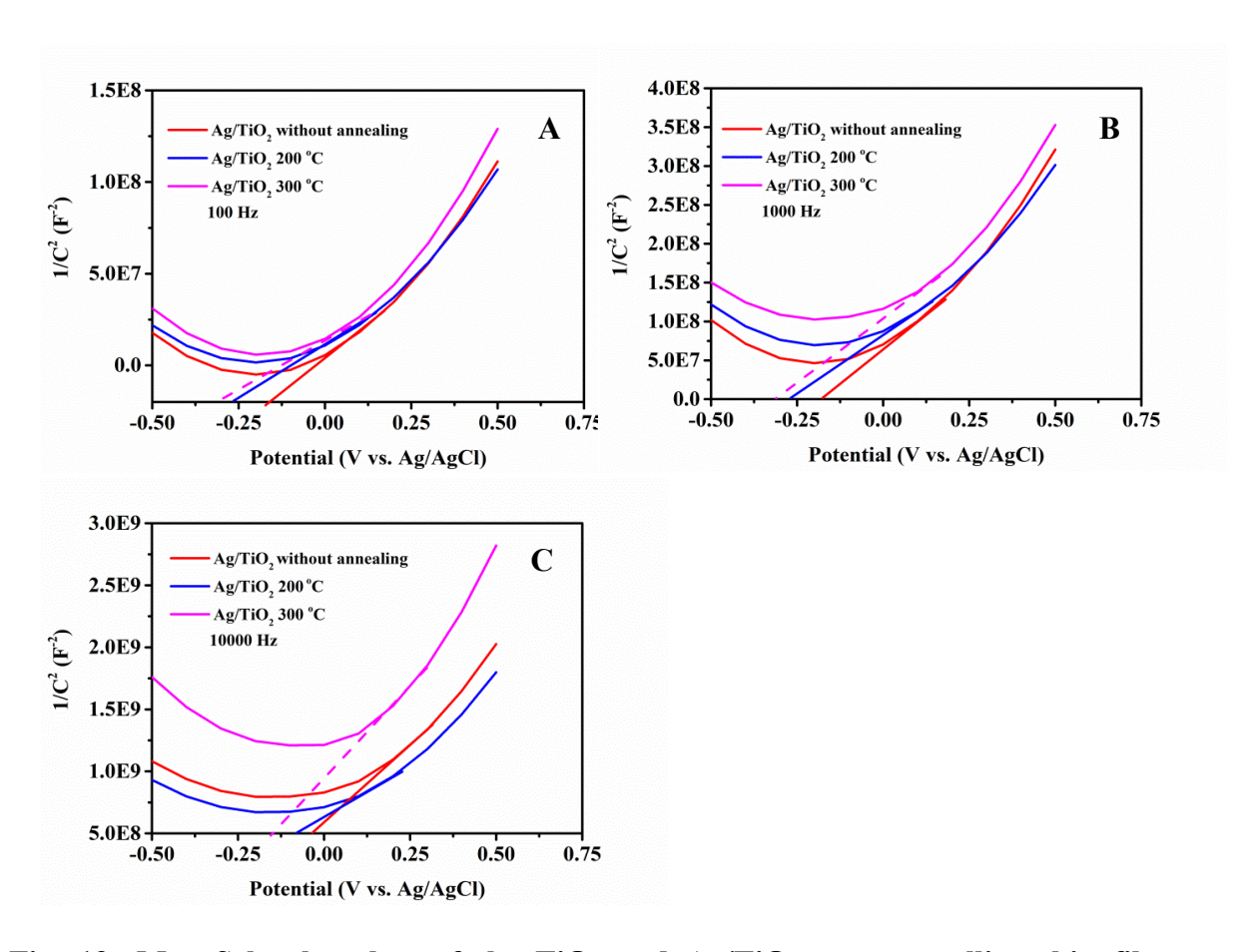


Fig. 13: Mott-Schottky plots of the TiO₂ and Ag/TiO₂ nanocrystalline thin films at a frequency of (A) 100 Hz, (B) 1000 Hz, and (C) 10000 Hz in the dark

Table 1: Obtained Mott-Schottky parameters of thin films nanostructures at a frequency of 100 Hz

Sample	N _D (cm ⁻	$ m V_{FB}$	W (nm)	$E_F(eV)$	E _{CB} (eV)	E _{VB} (eV)	L _D (cm)
	3)	(V)					
Ag/TiO ₂ as	9.6×10^{21}	-0.17	0.69	2.8×10^{-20}	-1.345	-4.745	$2x10^{-8}$
prepared							
Ag/TiO ₂	1.1×10^{22}	-0.27	0.76	4.3x10 ⁻²⁰	-1.349	-4.449	1.4x10 ⁻⁸
200°C							
Ag/TiO ₂	9.4×10^{21}	-0.32	0.87	5.1×10^{-20}	-1.345	-4.015	1.5×10^{-8}
300°C							

Table 2: Obtained Mott-Schottky parameters of thin films nanostructures at frequency of 1000 Hz

Sample	N_D (cm ⁻³⁾	$V_{FB}(V)$	W (nm)	$E_F(eV)$	E _{CB} (eV)	E _{VB} (eV)	L _D (cm)
Ag/TiO ₂ as	4.1×10^{21}	-0.18	1.07	$2.9x10^{-20}$	-1.323	-4.723	$2.3x10^{-8}$
prepared							
	21			20			0
Ag/TiO ₂	4.9×10^{21}	-0.27	1.13	4.2×10^{-20}	-1.328	-4.428	2.1x10 ⁻⁸
200°C							
Ag/TiO ₂	$4.7x10^{21}$	-0.32	1.23	2.0x10 ⁻²⁰	-1.327	-3.997	2.2x10 ⁻⁸
300°C							

Table 3: Obtained Mott-Schottky parameters of thin films nanostructures at frequency of 10000 Hz

Sample	N_D (cm ⁻³⁾	$V_{FB}(V)$	W (nm)	$E_F(eV)$	E_{CB}	E_{VB}	L _D (cm)
Ag/TiO ₂ as	1.0×10^{21}	-0.03	1.46	4x10 ⁻²¹	-1.287	-4.687	5x10 ⁻⁸
prepared							
Ag/TiO ₂	1.1×10^{21}	-0.08	1.67	1.3x10 ⁻²⁰	-1.289	-4.389	$5x10^{-8}$
200°C							
Ag/TiO ₂	9.5×10^{20}	-0.15	2.12	2.5x10 ⁻²⁰	-1.285	-3.955	5x10 ⁻⁸
300°C							

4. Conclusions

TiO₂ thin films were prepared by the CBD method. The films were coated by Ag NPs prepared by electrochemical techniques to prepare Ag/TiO₂ nanocrystalline thin films. MB dye was used to assess the films' photocatalytic efficacy in both low-intensity white light and sunlight. The degradation rate of the MB dye was found to be greater at a pH of 10 in comparison to a pH of 6. Moreover, the degrading efficiency exhibited a significant improvement, rising from 85% to 96%, after subjecting the Ag/TiO₂ nanocrystalline thin films to annealing at a temperature of 300 °C for a duration of 1 hour, followed by exposure to white light for a total of 240 minutes. The nanocrystalline thin films composed of Ag/TiO₂ demonstrated comparable photocatalytic performance when exposed to sunlight. However, the degradation rate is faster when compared to white light. Significantly, the MB dye was completely broken down at a pH of 10 in the presence of sunlight in about 150 min. The Ag/TiO₂ nanocrystalline photoelectrodes demonstrated faradaic performance, as evidenced by cyclic voltammetry (CV) measurements done in the absence of light. The Ag/TiO₂ photoanodes underwent Mott-Schottky analysis, revealing negative flat band potential (V_{FB}) values. This is consistent with the Nernst equation and indicates efficient separation of light-induced charges and enhanced efficiency in the process of splitting water. The donor density (N_D) of the Ag/TiO2 photoanodes was seen to have a higher value at a frequency of 100 Hz compared to frequencies of 1000 Hz and 10000 Hz. At a frequency of 10000 Hz, the process

of metallization causes a decrease in the depletion region, resulting in a reduction in the density of photocurrent.

References

- [1] A. Verma, P. Chaudhary, R. K. Tripathi, B. C. Yadav, Transient photodetection studies on 2D ZnO nanostructures prepared by simple organic-solvent assisted route, Sens. Actuators A Phys., 321(2021)112600, https://doi.org/10.1016/j.sna.2021.112600
- [2] B. P. Narasaiah, S. Koppala, P. Kar, B. Lokesh, B. K. Mandal, Photocatalytic and Antioxidant Studies of Bioinspired ZrO₂ Nanoparticles Using Agriculture Waste Durva Grass Aqueous Extracts, J. Hazard. Mater. Adv., 7 (2022) 100112, https://doi.org/10.1016/j.hazadv.2022.100112
- [3] J. J. Hassan, M. A. Mahdi, C. W. Chin, H. Abu-Hassan, Z. Hassan, Fabrication of ZnO nanorod/p-GaN high-brightness UV LED by microwave-assisted chemical bath deposition with Zn(OH)₂-PVA nanocomposites as seed layer, Opt. Mater., 35 (2013) 1035–1041, https://doi.org/10.1016/j.optmat.2012.12.006
- [4] J. J. Hassan, M. A. Mahdi, C. W. Chin, H. Abu-Hassan, Z. Hassan, A high-sensitivity room-temperature hydrogen gas sensor based on oblique and vertical ZnO nanorod arrays, Sens. Actuators B Chem., 176 (2013) 360–367, https://doi.org/10.1016/j.snb.2012.09.081
- [5] A. Hidayat, A. Taufiq, Z.A.I. Supardi, S.M. Jayadininggar, U. Sa'adah, N.A. Astarini, T. Suprayogi, M. Diantoro, Synthesis and characterization of TiO₂/ZnO-Ag@TiO₂ nanocomposite and their performance as photoanode of organic Dye-Sensitized Solar Cell, Mater. Today Proc., 44 (2021) 3395-3399, https://doi.org/10.1016/j.matpr.2020.11.862
- [6] L. Roza, Y. Febrianti, S. Iwan, V. Fauzia, The role of cobalt doping on the photocatalytic activity enhancement of ZnO nanorods under UV light irradiation, Surfaces and Interfaces, 18 (2020) 100435, https://doi.org/10.1016/j.surfin.2020.100435
- [7] F. Allawi, M. A. Mahdi, M. J. Kadhim, A. H. Omran Alkhayatt, Preparation and characterization of ZnO/CuO nanocomposites thin films for highly efficient visible-light photocatalysis of acriflavine dye, Optik, 303 (2024) 171722, https://doi.org/10.1016/j.ijleo.2024.171722
- [8] M. J. Kadhim, M. A. Mahdi, J. J. Hassan, H. H. Inaya, Z. A. Awad, A simple method to prepare and characterize ZnO/V₂O₅ nanostructure thin films for photoelectrochemical and photocatalytic uses in visible light, Phys. Scr., 99 (2024) 085524, https://doi.org/10.1088/1402-4896/ad5fc9
- [9] A. Ziashahabi, M. Prato, Z. Dang, R. Poursalehi, N. Naseri, The effect of silver oxidation on the photocatalytic activity of Ag/ZnO hybrid plasmonic/metal-oxide nanostructures under

- visible light and in the dark, Sci. Rep., 9 (2019) 48075, https://doi.org/10.1038/s41598-019-48075-7
- [10] Z. Zhang, Yuhang Ma, Xiaohai Bu, Qiong Wu, Zusheng Hang, Zhao Dong, Xiaohan Wu, Facile one-step synthesis of TiO₂/Ag/SnO₂ ternary heterostructures with enhanced visible light photocatalytic activity, Sci. Rep., 8 (2018) 28832, https://doi.org/10.1038/s41598-018-28832-w
- [11] Z. Chu, L. Qiu, Y. Chen, Z. Zhuang, P. Du, J. Xiong, TiO₂-loaded carbon fiber: Microwave hydrothermal synthesis and photocatalytic activity under UV light irradiation, J. Phys. Chem. Solids, 136 (2020) 109138, https://doi.org/10.1016/j.jpcs.2019.109138
- [12] S. Deka, P. A. Joy, Electronic structure and ferromagnetism of polycrystalline $Zn_{1-x}Co_xO$ (0 $\leq x \leq 0.15$), Solid State Commun., 134 (2005) 665–669, https://doi.org/10.1016/j.ssc.2005.03.013
- [13] J. Singh, K. Sahu, S. Mohapatra, Thermal annealing induced evolution of morphological, structural, optical and photocatalytic properties of Ag-TiO₂ nanocomposite thin films, J. Phys. Chem. Solids, 129 (2019) 317–323, https://doi.org/10.1016/j.jpcs.2019.01.034
- [14] N. Naseri, H. Kim, W. Choi, A. Z. Moshfegh, Optimal Ag concentration for H₂ production via Ag:TiO₂ nanocomposite thin film photoanode, Int. J. Hydrogen Energy, 37 (2012) 3056–3065, https://doi.org/10.1016/j.ijhydene.2011.11.041
- [15] D. Komaraiah, E. Radha, J. Sivakumar, M. V. Ramana Reddy, R. Sayanna, Photoluminescence and photocatalytic activity of spin coated Ag⁺ doped anatase TiO₂ thin films, Opt. Mater., 108 (2020) 110401, https://doi.org/10.1016/j.optmat.2020.110401
- [16] D. Chaudhary, S. Singh, V. D. Vankar, N. Khare, A ternary Ag/TiO₂/CNT photoanode for efficient photoelectrochemical water splitting under visible light irradiation, Int. J. Hydrogen Energy, 42 (2017) 7826–7835, https://doi.org/10.1016/j.ijhydene.2016.12.036
- [17] M. J. Kadhim, M. Mahdi, J. J. J. Hassan, A. S. Al-Asadi, Photocatalytic activity and photoelectrochemical properties of Ag/ZnO core/shell nanorods under low-intensity white light irradiation, Nanotechnology, 32 (2021) 195706, DOI 10.1088/1361-6528/abe3b3
- [18] A. M. Selman, Z. Hassan, M. Husham, Structural and photoluminescence studies of rutile TiO₂ nanorods prepared by chemical bath deposition method on Si substrates at different pH values, Measurement, 56 (2014) 155–162, https://doi.org/10.1016/j.measurement.2014.06.027
- [19] M. J. Kadhim, M. A. Mahdia, A. M. Selman, S. K. Jamel Al-Ani, J. J. Hassan, N. M. Ahmed, The most important parameters that affect the photocatalytic activity of ZnO nanostructures against organic dyes: A Review, Iran. J. Catal., 13 (2023) 1–21, https://doi.org/10.30495/ijc.2023.1969439.1966

- [20] H. Y. Jung, I. S. Yeo, T. U. Kim, H. C. Ki, H. B. Gu, Surface plasmon resonance effect of silver nanoparticles on a TiO₂ electrode for dye-sensitized solar cells, Appl. Surf. Sci., 432 (2018) 266–271, https://doi.org/10.1016/j.apsusc.2017.04.237
- [21] R. Singh, M. Kumar, M. Saini, A. Singh, B. Satpati, T. Som, Growth of TiO₂ thin films on chemically textured Si for solar cell applications as a hole-blocking and antireflection layer, Appl. Surf. Sci., 418 (2017) 225–231, https://doi.org/10.1016/j.apsusc.2017.01.307
- [22] D. Raval, M. Jani, H. Chaliyawala, A. Joshi, I. Mukhopadhyay, A. Ray, Solar to chemical energy conversion using titania nanorod photoanodes augmented by size distribution of plasmonic Au-nanoparticles, Mater. Chem. Phys., 231 (2019) 322–334, https://doi.org/10.1016/j.matchemphys.2019.04.025
- [23] B. K. Mehta, M. Chhajlani, B. D. Shrivastava, Green synthesis of silver nanoparticles and their characterization by XRD, J. Phys.: Conf. Ser., 836 (2017) 012050, https://doi.org/10.1088/1742-6596/836/1/012050
 - [24] C. Noberi, F. Kaya, C. Kaya, Synthesis, structure, characterization of hydrothermally synthesized Ag-TiO₂ nano-structures onto Ni filters using electrophoretic deposition, Ceramics International, 42(2016) 17202-17209, https://doi.org/10.1016/j.ceramint.2016.08.012
- [25] S. Raghu, C. W. Lee, S. Chellammal, S. Palanichamy, C. A. Basha, Evaluation of electrochemical oxidation techniques for degradation of dye effluents—A comparative approach, J. Hazard. Mater., 171 (2009) 748–754, https://doi.org/10.1016/j.jhazmat.2009.06.063
- [26] J. Akikusa, S. U. M. Khan, Photoresponse and AC impedance characterization of n-TiO₂ films during hydrogen and oxygen evolution reactions in an electrochemical cell, Int. J. Hydrogen Energy, 22 (1997) 875–882, https://doi.org/10.1016/S0360-3199(96)00235-2
- [27] M. Li, Y. Yang, Y. Ling, W. Qiu, F. Wang, T. Liu, Y. Song, X.-X. Liu, P.-P. Fang, Y. Tong, Y. Li, Morphology and doping engineering of Sn-doped hematite nanowire photoanodes, Nano Lett., 17 (2017) 2490–2495, https://doi.org/10.1021/acs.nanolett.7b00184
- [28] K. Kusdianto, D. Jiang, M. Kubo, M. Shimada, Effect of annealing temperature on the photocatalytic activity of Ag–TiO₂ nanocomposite films by one-step gas-phase deposition, Mater. Res. Bull., 101 (2018) 19–26, https://doi.org/10.1016/j.materresbull.2017.08.062
- [29] P. Sangpour, F. Hashemi, A. Z. Moshfegh, Photoenhanced Degradation of Methylene Blue on Cosputtered M:TiO₂ (M = Au, Ag, Cu) Nanocomposite Systems: A Comparative Study, J. Phys. Chem. C, 114 (2010) 13955–13961, https://doi.org/10.1021/jp910454r
- [30] Q. Feng, S. Li, W. Ma, H.-J. Fan, X. Wan, Y. Lei, Z. Chen, J. Yang, B. Qin, Synthesis and characterization of Fe₃O₄/ZnO-GO nanocomposites with improved photocatalytic

- degradation methyl orange under visible light irradiation, J. Alloys Compd., 737 (2018) 197–206, https://doi.org/10.1016/j.jallcom.2017.12.070
- 31] M. J. Kadhim, M. A. Mahdi, J. J. Hassan, Influence of pH on the photocatalytic activity of ZnO nanorods, Mater. Int., 2 (2020) 64–72, https://doi.org/10.1007/s10854-016-4284-0
- [32] T. Ngoc, T. Le, N. Quy, T. Ton, V. M. Tran, N. D. Nam, T. H. T. Vu, TiO₂ Nanotubes with Different Ag Loading to Enhance Visible-Light Photocatalytic Activity, Journal of Nanomaterials 2017 (2017) 7 https://doi.org/10.1155/2017/6092195
- [33] A. Shet, V. S. K, Solar light mediated photocatalytic degradation of phenol using Ag core—TiO₂ shell (Ag@TiO₂) nanoparticles in batch and fluidized bed reactor, Solar Energy, 127 (2016) 67–78, https://doi.org/10.1016/j.solener.2015.12.049
- [34] J. Singh, B. Satpati, S. Mohapatra, Structural, Optical and Plasmonic Properties of Ag-TiO2 Hybrid Plasmonic Nanostructures with Enhanced Photocatalytic Activity, *Plasmonics*, 12 (2017), 877–888, https://doi:10.1007/s11468-016-0339-6.
- [35] M. 'Aravind, M. Armanalanathan, S. Aslam, A. E. Noor, D. Jini, S. Majeed, P. Velusamy, Asma A. Alothman, R. A. Alshgari, M. S. S. Mushab, M. Sillanpaa, Hydrothermally Synthesized Ag-TiO2 nanofibers (NFS) for photocatalytic dye degradation and antibacterial activity, *Chemosphere*, 321(2023), 138077, https://doi.org/10.1016/j.chemosphere.2023.138077.
- [36] G. Preethi, R. Balan, S. Koppala, H. P. Nagaswarupa, Cubic and orthorhombic Cd₂SnO₄ microcrystals: Molten salt synthesis, phase evolution and dye degradation studies, Mater. Res. Express, 6 (2019) 105010, https://doi.org/10.1088/2053-1591/ab406f
 - [37] S. Koppala, R. Balan, I. Banerjee, K. Li, L. Xu, H. Liu, D. K. Kumar, K. R. Reddy, V. Sadhu, Room temperature synthesis of novel worm like tin oxide nanoparticles for photocatalytic degradation of organic pollutants, Mater. Sci. Energy Technol., 4 (2021) 113–118, https://doi.org/10.1016/j.mset.2021.03.002
- [38] S. Koppala, Y. Xia, L. Zhang, J. Peng, Z. Chen, L. Xu, Hierarchical ZnO/Ag nanocomposites for plasmon-enhanced visible-light photocatalytic performance, Ceram. Int., 45 (2019) 15116–15121, https://doi.org/10.1016/j.ceramint.2019.04.252
 - [39] C. Clavero, Plasmon-induced hot-electron generation at nanoparticle/metal-oxide interfaces for photovoltaic and photocatalytic devices, Nat. Photonics, 8 (2014) 95–103, https://doi.org/10.1038/nphoton.2013.238
- [40] R. Gang, Y. Xia, L. Xu, L. Zhang, S. Ju, Z. Wang, S. Koppala, Size controlled Ag decorated TiO₂ plasmonic photocatalysts for tetracycline degradation under visible light, Surfaces and Interfaces, 31 (2022) 102018, https://doi.org/10.1016/j.surfin.2022.102018

- [41] X. H. Yang, H. T. Fu, X. C. Wang, J. L. Yang, X. C. Jiang, A. B. Yu, Synthesis of silver-titanium dioxide nanocomposites for antimicrobial applications, J. Nanopart. Res., 16 (2014) 2526–2537, https://doi.org/10.1007/s11051-014-2526-8
- [42] K. K. Paul, P. K. Giri, Role of Surface Plasmons and Hot Electrons on the Multi-Step Photocatalytic Decay by Defect Enriched Ag@TiO2 Nanorods under Visible Light, J. Phys. Chem. C, 121 (2017) 20016–20030, https://doi.org/10.1021/acs.jpcc.7b05328
- [43] A. S. Al-Asadi, L. A. Henley, M. Wasala, B. Muchharla, N. Perea-Lopez, V. Carozo, Z. Lin, M. Terrones, K. Mondal, K. Kordas, S. Talapatra, Aligned carbon nanotube/zinc oxide nanowire hybrids as high performance electrodes for supercapacitor applications, J. Appl. Phys., 121 (2017) 124303, https://doi.org/10.1063/1.4979098
- [44] H.Qi, Z. Bo, S. Yang, L. Duan, H. Yang, J. Yan, K. Cen, K. Ostrikov, Hierarchical nanocarbon-MnO2 electrodes for enhanced electrochemical capacitor performance, Energy Storage Mater., 16 (2019) 607–618, https://doi.org/10.1016/j.ensm.2018.07.019
- [45] P. R. Deshmukh, Y. Sohn, W. G. Shin, Chemical synthesis of ZnO nanorods: Investigations of electrochemical performance and photo-electrochemical water splitting applications, J. Alloys Compd., 711 (2017) 573–580, https://doi.org/10.1016/j.jallcom.2017.04.030
- [46] Y. Qiu, K. Yan, H. Deng, S. Yang, Secondary branching and nitrogen doping of ZnO nanotetrapods: building a highly active network for photoelectrochemical water splitting, Nano Lett., 12 (2012) 407–413, https://doi.org/10.1021/nl2037326
- [47] I. S. Cho, Z. Chen, A. J. Forman, D. R. Kim, P. M. Rao, T. F. Jaramillo, X. Zheng, Branched TiO2 Nanorods for Photoelectrochemical Hydrogen Production, Nano Lett., 11 (2011) 4978–4984, https://doi.org/10.1021/nl2029392
- [48] K. S. Raja, V. K. Mahajan, M. Misra, Determination of photo conversion efficiency of nanotubular titanium oxide photo-electrochemical cell for solar hydrogen generation, *J Power Sources*, 159 (2006), 1258–1265, https://doi.org/10.1016/j.jpowsour.2005.12.036.
 - [49] W.-D. Zhang, L.-C. Jiang, J.-S. Ye, Photoelectrochemical study on charge transfer properties of ZnO nanowires promoted by carbon nanotubes, J. Phys. Chem. C, 113 (2009) 16247–16253, https://doi.org/10.1021/jp905500n
 - [50] A. Lamberti, ZnO- and TiO2-Based Nanostructures, *Nanomaterials* **2018**, *8*(5), 325, https://doi.org/10.3390/nano8050325
 - [51] N. D. Sankir, M. Sankir, Photoelectrochemical Solar Cells, John Wiley & Sons, 2018.
 - [52] J. Alexander, Surface modifications and growth of titanium dioxide for photo-electrochemical water splitting, Doctoral Thesis, Imperial College London, UK, Springer International Publishing Switzerland, 2016.

- [53] D. Ramírez-Ortega, A. M. Meléndez, P. Acevedo-Peña, I. González, R. Arroyo, Semiconducting properties of ZnO/TiO2 composites by electrochemical measurements and their relationship with photocatalytic activity, Electrochim. Acta, 140 (2014) 541–549, https://doi.org/10.1016/j.electacta.2014.06.060
- [54] T. Lee, H. Ryu, W. Lee, Photoelectrochemical properties of iron (III)-doped TiO2 nanorods, Ceram. Int., 41 (2015) 7582–7589, https://doi.org/10.1016/j.ceramint.2015.02.082
- [55] F. Rasouli, A. Rouhollahi, F. Ghahramanifard, Fabrication of silver nanoparticles decorated zinc oxide nanotubes by electrodeposition technique for photoelectrochemical water splitting, Mater. Sci. Semicond. Process., 93 (2019) 371–378, https://doi.org/10.1016/j.mssp.2018.08.004
- [56] R. G. Freitas, M. A. Santanna, E. C. Pereira, Preparation and characterization of TiO2 nanotube arrays in ionic liquid for water splitting, Electrochim. Acta, 136 (2014) 404–411, https://doi.org/10.1016/j.electacta.2014.05.097
- [57] P. Sahoo, A. Sharma, S. Padhan, G. Udayabhanu, R. Thangavel, UV-assisted water splitting of stable Cl-doped ZnO nanorod photoanodes grown via facile sol-gel hydrothermal technique for enhanced solar energy harvesting applications, Solar Energy, 193 (2019) 148–163, https://doi.org/10.1016/j.solener.2019.09.045
- [58] B. Xin, Z. Ren, H. Hu, X. Zhang, C. Dong, K. Shi, L. Jing, H. Fu, Photocatalytic activity and interfacial carrier transfer of Ag-TiO2 nanoparticle films, Appl. Surf. Sci., 252 (2005) 2050–2055, https://doi.org/10.1016/j.apsusc.2005.03.172

المحفز الضوئي والخلية الكهروضوئية للأغشية Ag/TiO_2 الرقيقة النانوية التركيب تحت ضوء مرئي منخفض الشدة

 2 مروة جواد كاظم 1 و مازن عوني مهدي 1 و جلال جبار حسن 1 و سلوان كمال جميل

1 قسم الفيزياء-كلية العلوم-جامعة البصرة-العراق

2 قسم الفيزياء-كلية العلوم-الجامعة المستنصرية-بغداد-العراق

المستخلص

تم تصنيع أغشية رقيقة نانوية التركيب من ثاني أكسيد التيتانيوم (TiO₂) باستعمال الترسيب الكيميائي على قواعد زجاجية و TiO₂ تم ترسيب جسيمات نانوية من الفضة (Ag) على سطح أغشية TiO₂ الرقيقة بالطرق الكهروكيميائية. تراوح حجم جسيمات الفضة النانوية على أغشية TiO₂ من 10 إلى 79 نانومتر على كل من قواعد الزجاج و FTO. تم تقييم كفاءة العينات المحضرة للتحفيز الضوئي للأغشية الرقيقة النانوية من Ag/TiO₂ ، سواء غير المعالجة أو المعالجة حرارياً عند 200 درجة مئوية و 300 درجة مئوية المدة ساعة واحدة، من خلال التحلل الضوئي لصبغة الميثيلين الزرقاء (MB) تحت الضوء الأبيض (0.33 ميلي واط/سم²) وأشعة الشمس. ومن اللافت للنظر أن أغشية TiO₂ الرقيقة المعالجة حرارياً عند 300 درجة مئوية حققت نسبة تحلل بلغت 96% بعد 240 دقيقة تحت الضوء الأبيض. تحت أشعة الشمس و عند درجة حامضية 10، وصلت نسبة التحلل إلى 100% خلال 150 دقيقة. كشف قياس الجهد الدوري عن سلوك فاراداي في الأغشية الرقيقة Ag/TiO₂. حُددت كفاءة التحويل الضوئي (n) للأغشية، المقاسة في حالتها المُحضرة وبعد المعالجة الحرارية عند 200 درجة مئوية، بأنها 1.5% و 1.6% و 0.5% على التوالي. حالتها المُحضرة وبعد المعالجة الحرارية عند 200 درجة مئوية، بأنها 1.5% و 1.6% و 0.5% على التوالي. أكد تحليل موت-شوتكي السلوك من النوع n ، وأشار إلى انزياح سلبي في جهد النطاق المسطح (V_{FB}).

الكلمات المفتاحية: Ag/TiO₂؛ أغشية رقيقة ؛ حفّازات ضوئية ؛ خلية كهروكيميائية ضوئية.